Optica Applicata, Vol. LV, No. 2, 2025
DOI: 10.37190/oa/201188

Optimization of parameters for skin cancer diagnostics using reflected terahertz radiation

M. Milosevic, N. Stevanovic*, V.M. Markovic

Faculty of Science, University of Kragujevac,
12 R. Domanovica Street, 34000 Kragujevac, Serbia

*Corresponding author: nenad.stevanovic@pmf.kg.ac.rs

In this paper, the reflected THz radiation from the healthy skin and skin affected by cancer was analyzed. For that purpose, finite difference time domain (FDTD) method for electromagnetic wave propagation was adjusted and applied to simulate THz radiation propagation according to the human skin. Here, radiation from 0.1 to 1 THz was considered. Multi-layer skin model was applied with given electric parameters for each skin layer. The parameters used were conductivity and dielectric constant. The values of parameters depend on frequency and highly depend on whether the skin is healthy or not.

It was found that the intensity of reflected radiation from the cancerous skin is greater than the intensity of reflected radiation from the healthy skin, and that the difference between these two intensities increases with increasing frequency. It was also obtained that the distribution of reflected radiation is similar to the distribution of incident radiation, while absorption of transmitted radiation is very small. These results obtained within this paper are significant because they indicate that the reflected radiation from the skin could be used for skin cancer diagnostics.

Keywords: skin, terahertz radiation, cancer, FDTD method.

1. Introduction

The human organ with the largest mass, 15% of the total human body, and the largest surface (1.8 m^2) is the skin. The depth of the skin is from 0.2 up to 4 mm. The skin consists of three layers: the epidermis, the dermis, and the hypodermis [1-3].

The epidermis is the outer layer of the skin, which can be further divided into sub-layers (from the surface to the inside of the body): stratum corneum, stratum granulosum, stratum spinosum, and stratum basale. The epidermis is a semi-permeable membrane. Its functions serve to protect the body from the external environment. It contributes to the maintenance of moisture in the body and continuously creates new skin cells. The dermis, located below the epidermis, is the thickest layer of the skin. Its components are collagen, elastic fibers, and extrafibrillar matrix. The main functions of the dermis are to regulate body temperature and supply the epidermis with nutrients. It contains nerve receptors for touch and pain. The hypodermis is the deepest inner layer of the skin, which is made up of fat cells, connective tissue, and blood

vessels. Among other things, the hypodermis protects the body from external shocks, connects the skin with muscles and bones, and plays a role in body temperature regulation [4-8].

Many papers have been published on the structure and properties of the skin using non-ionizing radiation with a frequency of several GHz and THz, which has led to the development of various methods for the diagnostics and treatment of skin diseases [9-14]. The skin with malignant tissue contains a different percentage of water compared to the healthy skin [9] and, as a consequence, the value of permittivity is different [10]. Similar results were obtained in [11] where the degree of skin hydration and human skin reflectance were investigated, using frequencies from 80 to 100 GHz. In the paper [12], the authors used a radiometer with a central frequency of 90 GHz and a bandwidth of 20 GHz to measure the skin reflectance for the cases of healthy and diseased skin. They showed that there were significant differences in the reflectance of the skin between healthy and diseased parts of the skin, and they indicated the potential of using radiometry for the non-contact diagnostics of skin diseases. The authors of the paper [9] used a simple half-space electromagnetic model to measure (using a 95 GHz radiometer) and perform simulations (in the range from 30 to 100 GHz, for several different skin water contents: 50% – dry, 75% – normal healthy, 95% – skin with malignant lesions) to determine the emissivity of the skin. They showed that the emissivity of the skin increases with increasing frequency and with decreasing water content in the skin. In addition to the reflected waves, transmitted ones are investigated in papers [13,14], where SAR was calculated for the frequency of up to 60 GHz. It was concluded in these papers that the largest values of energy radiation are absorbed in the epidermis. This confirmed that radiometry could be used as a non-contact method for diagnosing and monitoring skin diseases.

Several non-invasive methods have been developed for the diagnosis of skin cancer, such as optical coherence tomography, Raman spectroscopy, dermoscopy, ultrasound, *etc*. Optical coherence tomography (OCT) method works on the principle of interference (Michelson interferometry) infrared light. Namely, the source emits light that is split into two parts. One part of the light is directed to the skin, and the other part to the reference mirror. The light reflected from the skin is combined with the light reflected from the reference mirror forming an interference pattern that is detected and based on that an image of the internal structure is formed. The OCT method provides high-resolution images of structure superficial layers of the skin *in vivo* in real-time, and it can be used up to 1 to 2 mm depth with a resolution between 3 and 15 μm. The disadvantages of this method are that it is not able to examine the deeper layers of the skin in detail, insufficient accuracy in early detection of cancer, and that OCT devices can be expensive. Raman spectroscopy is a method of analysis which provides detailed information about chemical structure, phase, polymorphism and molecular interactions within the sample. In this method, monochromatic laser radiation (visible, or near infrared/UV radiation) of high intensity is directed towards the sample (tissue), whereby the molecules of the sample scatter that radiation. Almost all scattered radiation has the same wavelength as the incident laser radiation and no information can

be obtained from it, however a very small part of the scattered radiation has a different wavelength than the incident radiation depending on the chemical structure of the sample (Raman scattering). A Raman spectrum contains a number of peaks, showing the intensity and wavelength position of the Raman scattered light, and each Raman spectrum is mostly different for different samples, so by comparing it with the data from the database, can determine which sample (molecule) is irradiated. Raman spectroscopy enables real-time analysis, whereby different types of cancer and other skin diseases can be distinguished, however, the spectra are complex, so the analysis can be complicated, and requires expensive devices, also the samples can be overheated due to the high intensity of the laser radiation. Dermoscopy is very suitable for distinguishing melanoma cells from BCC (Basal cell carcinoma) and SCC (Squamous cell carcinoma) with a high level of accuracy, however, it requires high-resolution cameras and highly trained personnel. Ultrasound is a painless method that is well tolerated by patients, can provide high-resolution visualization, and can be used to determine the depth of melanoma, but it is expensive equipment and requires experienced operators [15-18].

Several papers were published with application of THz radiation for investigation of skin characteristics [19-22]. Authors obtained that the electrical parameters of healthy and diseased skin differ significantly [19,21,23,24], whereby cancerous skin has higher values of relative electric constant and conductivity compared to healthy skin, at the same frequency [24,25]. In the paper [26], the authors used the FDTD method to simulate the passage of 0.45 THz radiation and concluded that, in the thin skin, the greatest amount of energy is absorbed in the first layer of the stratum spinosum. They also showed that the surface layer of the skin affects the reflection of radiation. In all these papers reflected radiation was used for determination of characteristics of the skin.

The goal of our work is by applying FDTD method examine how the distribution of reflected radiation changes with the change in the electrical parameters of the skin, and how it can be applied for determination is it skin healthy or not. In addition to electrical parameters, we will also take into account radiation conditions, geometry and frequency, and based on these parameters, we will evaluate the most optimal conditions that can be used in diagnostics.

2. Simulation of THz radiation on the skin with FDTD method

FDTD method [27-30] for the numerical simulation of propagation of electromagnetic (EM) waves is based on Maxwell's equations in differential form

$$-\sigma_{\mathrm{m}}\mathbf{H} - \mu\frac{\partial \mathbf{H}}{\partial t} = \nabla \times \mathbf{E} \tag{1}$$

$$\sigma\mathbf{E} + \varepsilon\frac{\partial \mathbf{E}}{\partial t} = \nabla \times \mathbf{H} \tag{2}$$

Here, $\mathbf{E}$ is the vector of the electric field, $\mathbf{H}$ is the vector of the magnetic field, μ and ε are magnetic permeability and electric permittivity, respectively, while σ is the elec-

tric conductivity of media and $\sigma_m = 0$ is magnetic conductivity. Propagation of the electric and magnetic field could be considered in two dimensions (2D), for example, a *xy*-plane in the Cartesian coordinate system. In this paper, transversal electric (TE) wave, where the electric field vector is normal to the *xOy* plane, was considered, using the sinusoidal wave source.

The TE mode sets up the electric field transverse to the direction of wave propagation, directed toward the *z*-axis. In this mode, three components of the EM field are considered, one component of the electric and two components of the magnetic field (H_x, H_y, E_z). Other components of the EM field are equal to zero. This corresponds to the S-polarization of THz radiation. The set of Eqs. (1) and (2) in scalar form becomes

$$-\mu \frac{\partial H_x}{\partial t} = \frac{\partial E_z}{\partial y} \tag{3}$$

$$\mu \frac{\partial H_y}{\partial t} = \frac{\partial E_z}{\partial x} \tag{4}$$

$$\sigma E_z + \varepsilon \frac{\partial E_z}{\partial t} = \frac{\partial H_y}{\partial x} - \frac{\partial H_x}{\partial y} \tag{5}$$

The first and second equations give the derivation of the magnetic field over time, being proportional to the derivation of the electric field over spatial coordinates. Conversely, the third equation gives the derivation of the electric field over time, being proportional to the derivation of the magnetic field over spatial coordinates. These equations can be transformed in finite difference notation introducing a time and space grid. In discretized form, Eqs. (3)–(5) take the form [30]

$$H_x^{q+\frac{1}{2}}[m, n] = H_x^{q-\frac{1}{2}}[m, n] - \frac{\Delta t}{\mu \Delta y}\left(E_z^q[m, n+1] - E_z^q[m, n]\right) \tag{6}$$

$$H_y^{q+\frac{1}{2}}[m, n] = H_y^{q-\frac{1}{2}}[m, n] + \frac{\Delta t}{\mu \Delta x}\left(E_z^q[m+1, n] - E_z^q[m, n]\right) \tag{7}$$

$$\begin{aligned} E_z^{q+1}[m, n] = {} & \frac{1 - \frac{\sigma \Delta t}{2\varepsilon}}{1 + \frac{\sigma \Delta t}{2\varepsilon}} E_z^q[m, n] \\ & + \frac{1}{1 + \frac{\sigma \Delta t}{2\varepsilon}} \frac{\Delta t}{\varepsilon \Delta x}\left(H_y^{q+\frac{1}{2}}[m, n] - H_y^{q+\frac{1}{2}}[m-1, n]\right) \\ & - \frac{1}{1 + \frac{\sigma \Delta t}{2\varepsilon}} \frac{\Delta t}{\varepsilon \Delta y}\left(H_x^{q+\frac{1}{2}}[m, n] - H_x^{q+\frac{1}{2}}[m, n-1]\right) \end{aligned} \tag{8}$$

where Δx and Δy denote spatial steps are between successive points in x and y coordinates and Δt is the time step. Indexes, m, n correspond to spatial and q to time coordinates. In this paper, a square grid is introduced, where $\Delta = \Delta x = \Delta y$. This method was successfully applied to light propagation through inhomogeneous and conductive media with different geometry of the source [31]. By discretizing the equations, coordinates x and y are translated to the discrete coordinates m and n, respectively. In this way, the xOy plane in the Cartesian coordinate system was translated into mOn plane (Fig. 1). For each point of the grid, defined by the points with coordinates (m, n), the values of the medium characteristics are defined: electric conductivity $\sigma[m, n]$, electric permittivity $\varepsilon[m, n]$, and magnetic permeability $\mu[m, n]$. If these values are equal at each point, then the medium is homogeneous; otherwise it is inhomogeneous. At the initial moment, $q = 0$ values of electric and magnetic field strength are set to zero at all points of the grid, except at the point of source. In the next time step, the values of fields are calculated using the values of fields in the previous time step, for each point (m, n) of the grid.

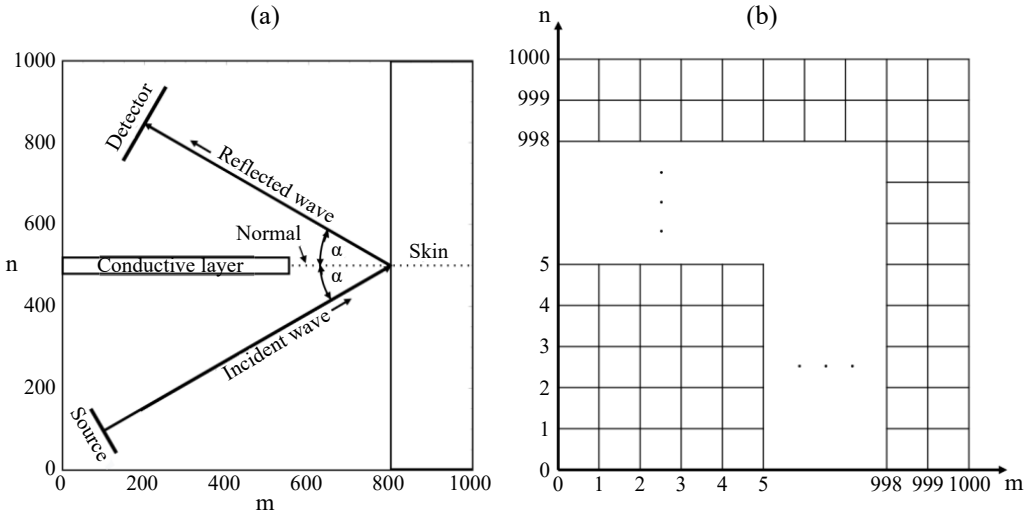

Fig. 1. (a) Geometry of source and skin in the *mOn* plane. (b) 2D grid in the *mOn* plane.

The shape of the source is the line, where each point of the source emits THz radiation with electric field strength as

$$E_z[m, n, t] = E_0 \cos(\omega t) \tag{9}$$

where $\omega = 2\pi / T$ and $E_0 = 100$ V/m is the electric field frequency and amplitude. The values of m and n are chosen that satisfy the equation of the line representing the source, $n = -m\,\mathrm{ctg}(\alpha) + b$, where α is the angle of direction of incident radiation in respect to normal on the skin and b depends on the position of the source. The distance of the source from the skin is several centimeters. The dimensions and shape of the source

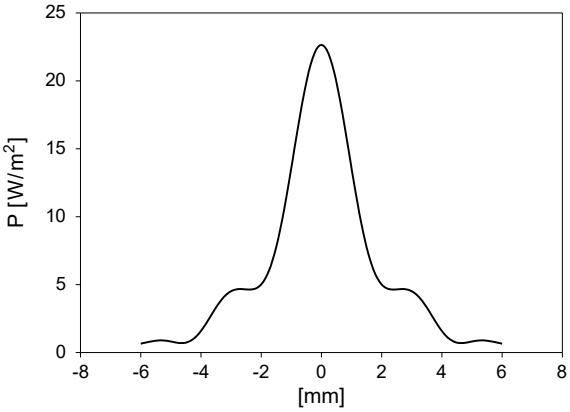

Fig. 2. Distribution of incident radiation on the skin surface.

and its distance from the skin influence the distribution of the incident radiation on the skin. Even though the source is homogenous, the distribution of incident radiation highly deviates from the homogenous distribution, as it is presented in Fig. 2.

The investigation carried out in this paper refers to frequencies in the range of 0.1–1 THz for radiation that changes harmonically at the source, forming plane electromagnetic wave. The distance of the source to the skin is the same as the distance of the detector to the skin and is several centimeters. This is the spatial limit at which the source and detector can be used to achieve presented results. The distribution of radiation from the source is homogeneous and harmonic with the assumption that a plane wave with linear polarized electric field is emitted, however, the wave front is deformed due to diffraction and the distribution of the intensity of the radiation which incident on the skin is shown in Fig. 2.

The skin is modeled as a medium of four layers with mutual parallel boundaries. Here, it is assumed that all layers are homogeneous, and their electric parameters depend on the frequency of radiation, which is presented in the Table. Besides electric parameters, the depth and density of skin layers are presented in the Table.

T a b l e. Dimensions and parameters of skin layers [26,32-35].

Skin layers	Relative electric constant and conductivity with different frequency						Density and depth	
	0.10 THz		0.55 THz		1.00 THz			
	ε_r	σ [S/m]	ε_r	σ [S/m]	ε_r	σ [S/m]	ρ [kg/m^3]	d [mm]
Stratum corneum	3.2	7.2	3.1	36.7	2.8	44.5	1200	0.25
Stratum spinosum	7.0	57.8	3.8	79.5	2.7	94.5	1060	0.1
Stratum basale	10.0	86.7	4.6	119.2	4.2	150.1	1060	0.05
Dermis	9.0	79.5	3.8	107.0	3.5	127.8	1080	2.0

The mentioned types of skin cancer occur in the first layers. As a result of cancer formation, the characteristics of the first layers of the skin will be changed, where values of electrical parameters increase by up to 30%. This change in parameters is enough that the reflected radiation from cancer skin has a higher intensity than the reflected radiation from healthy skin. Therefore, this method can be used as an indicator is there cancer in skin or not, but it is necessary to apply additional methods for determination of type of cancer.

To simulate THz radiation propagation according to the skin type, software in C^{++} language was developed. 2D grid was formed with dimensions of $m \times n$ number of elements as presented in Fig. 1(b). Numbers m and n can be arbitrarily taken. In this paper, m and n were set to 1000. The spatial step Δ depends on the wavelength and criteria in the literature is the tenth part of the value of λ. In this paper, the frequencies of radiation are in the range $f = (0.1, -1)$ THz, and the wavelength is calculated as set to $\lambda = c_0/f$ where c_0 is the speed of light in the vacuum. For this range of frequencies, it was chosen $\Delta = 6 \times 10^{-5}$ m. To fulfill the stability of the calculation, the time step must satisfy condition $\Delta t \leq \Delta/(2c_0)$. The number of time steps in the simulation is 4000 which corresponds to the total time of light propagation as equal to $4000\,\Delta t$. The time of the one light oscillation is $T = 1/f$.

The value of magnetic or electric field strength in the node (m, n) in time step $q + 1$ depends on the values of the field in that and adjacent elements in the previous time step time. When components of the electric and magnetic field in some moments of time are determined, the intensity of the THz radiation can be calculated as

$$I = \sqrt{\frac{\varepsilon_0}{\mu_0}}\,\langle E^2 \rangle \tag{10}$$

where $\langle E^2 \rangle$ presents the mean value of the square electric field component of reflected THz radiation over time for one period of oscillation given by

$$\langle E^2 \rangle = \frac{1}{T}\int_0^T E^2\,\mathrm{d}t \tag{11}$$

In this paper, integration in Eq. (11) was translated into sum as

$$\langle E^2 \rangle = \frac{1}{N}\sum_{k=1}^{N} E^2 \tag{12}$$

where N is the number of time steps during the one period of oscillation $N = T/\Delta t$.

3. Results and discussion

As noted in introduction section, many parameters affect reflected radiation. The first important parameter is the dielectric constant of the skin layers. In the layers of cancer skin, a greater amount of water is present, the concentration of atypical cells is higher, and the refractive index of these layers changes. The second important parameter is

the specific conductivity. Due to the greater amount of water in the layers of diseased skin, the specific conductivity increases, which reduces the propagation of incident radiation and increases reflected radiation. The density of the skin can also change, as can the appearance of inhomogeneous and heterogeneous structures in the layers of the skin. The thickness of the skin layers is a very important parameter. At these frequencies, radiation reaches only the first layers of the skin, and their characteristics are of great importance for this method. In this work, we took into account only the change in the electrical properties of the skin layers and examined their influence on reflected radiation.

Distributions of reflected THz radiation from the skin were determined for two cases: for angle $\alpha = 30°$ and for angle $\alpha = 45°$. These positions of the source with respect to the skin surface enable separation of the incident and reflected radiation and there is no mixture between them before and after the reflection. To eliminate the mixture along the normal to the skin surface, one thin and conductive layer was inserted with dimensions $550\Delta \times 40\Delta$ (Fig. 1(a)). The electrical parameters of the conductive layer are $\varepsilon_r = 1$ and $\sigma = 1$ MS/m.

For healthy skin, the parameters of the skin layers are presented in the Table. The parameters for cancerous skin have larger values compared to healthy skin. The difference in parameters can be larger than 30% [36,37]. In this paper, the relative electric constant and conductivity for cancer skin is 1.3 times higher than that for healthy skin. The distribution of reflected radiation was calculated on the line defined by the equation $n = m\,\mathrm{ctg}(\alpha) + b$.

Figure 3 shows the distribution of intensity of reflected radiation for $f = 0.1$ THz for angles $\alpha = 30°$ and $\alpha = 45°$, where the dimension of the step $\Delta = 6 \times 10^{-5}$ m. The ordinate shows the radiation intensity, based on Eqs. (10)–(12), while the position on the screen is shown on the abscissa. From the graph, it can be seen that the distributions of intensity have a similar shape and the difference between them is up to 10%. The intensity of reflected radiation from healthy skin for 30° is greater than the intensity of

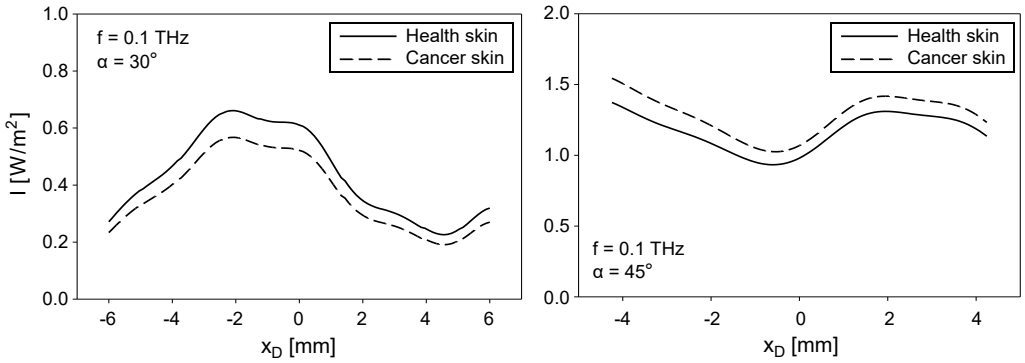

Fig. 3. Distribution of intensity of radiation with $f = 0.1$ THz with $\alpha = 30°$ and $\alpha = 45°$, as a function of position on the screen, $\Delta = 6 \times 10^{-5}$ m.

reflected radiation from cancerous skin. For an angle of 45°, it is the opposite. The intensity of reflected radiation for 45° is around 2 times higher than for 30° for both healthy and cancerous skin.

For the chosen step dimension, the distance from the center of the source to the skin is 3 cm, which, at a frequency of 0.1 THz, represents 10 wavelengths of emitted radiation. It is a very close zone and a much greater distance between the source and the skin is needed. The form of the distribution of incident radiation will not be as presented in Fig. 2. For the analysis of such a distribution of incident radiation, it is necessary to use larger distances. This can be achieved if a space with a much larger number of steps is considered, so the grid should consist of 5 000 × 5 000 elements. This significantly slows down the computation and simulation execution time. Another way is to increase the dimensions of the steps.

Figure 4 shows the distribution of intensity of reflected radiation for $f = 0.1$ THz for angles $\alpha = 30°$ and $\alpha = 45°$, where the dimension of the step $\Delta = 30 \times 10^{-5}$ m. At the graph on the right side, the case where parameters of the skin "modified" randomly for 10% in respect to parameters of cancer skin. It could be seen that small change of parameters strongly influences the intensity of reflected radiation. The intensity of reflected radiation is maximal at the center of the screen and decreases with distance. The shapes of the intensity distributions for both types of skin are the same. For both incident angles of radiation, the intensity of reflected radiation from the cancer skin is more than 2 times larger than it for healthy skin.

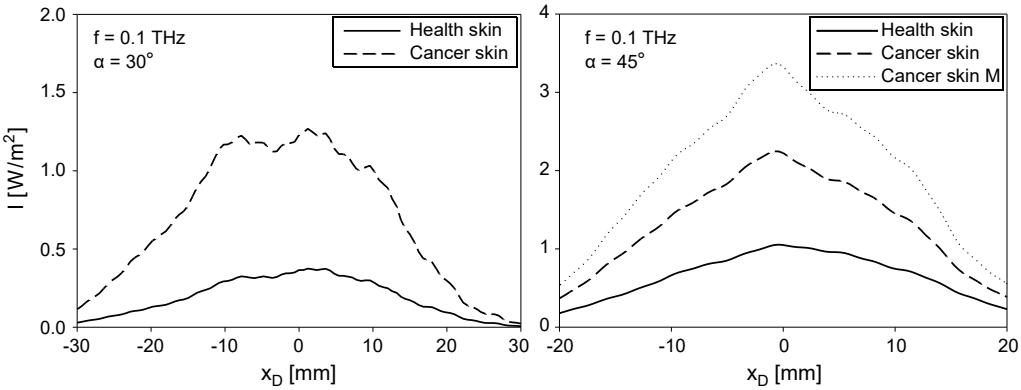

Fig. 4. Distribution of intensity of radiation with $f = 0.1$ THz with $\alpha = 30°$ and $\alpha = 45°$, as a function of position on the screen, $\Delta = 30 \times 10^{-5}$ m.

It is important to emphasize that the distribution of radiation intensity depends on the geometry of the source and its distance from the skin.

Figure 5 shows the distribution of intensity of reflected radiation for $f = 0.55$ THz for angles $\alpha = 30°$ and $\alpha = 45°$, where the dimension of the step $\Delta = 6 \times 10^{-5}$ m. It is clear that the intensity of reflected radiation is maximal at the center of the screen and decreases with distance. The shapes of the intensity distributions for both types of skin

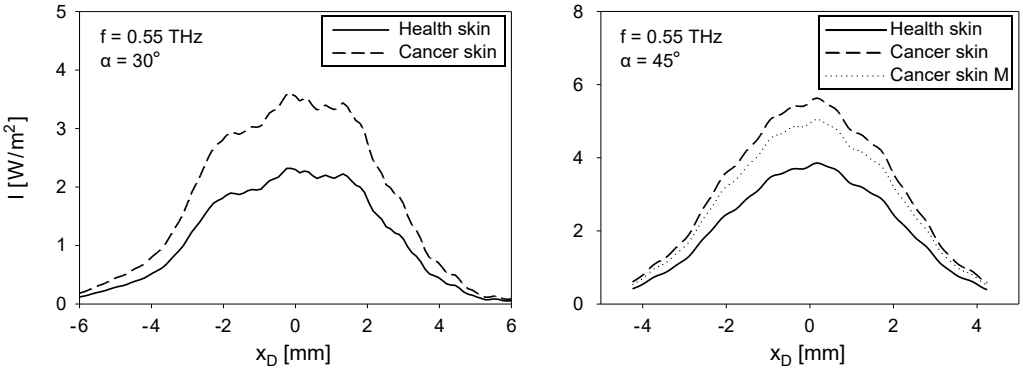

Fig. 5. Distribution of intensity of radiation with $f = 0.55$ THz with $\alpha = 30°$ and $\alpha = 45°$, as a function of position on the screen, $\Delta = 6 \times 10^{-5}$ m.

are the same. For both incident angles of radiation, the intensity of reflected radiation from the cancerous skin is larger, especially at the center of the screen where the difference is up to 50%.

As in a previous case, at the graph on the right side, the intensity of reflected radiation was presented for modified parameters and it could be seen that their influence is not strong. It means that higher frequency of radiation enables better diagnostic.

Figure 6 shows the distribution of intensity of reflected radiation for $f = 1$ THz for angles $\alpha = 30°$ and $\alpha = 45°$, where the dimension of the step $\Delta = 6 \times 10^{-5}$ m. Distributions of radiation intensity are narrow and the majority of reflected radiation is at the center of the screen. For both incident angles of radiation, the intensity of reflected radiation from the cancerous skin is up to 2 times larger at the center of the screen.

It is important to see that modified parameters of the skin do not influence the intensity of reflected radiation and this frequency is the best for diagnostic. Higher frequency has more reliability and precision for determination of skin parameters.

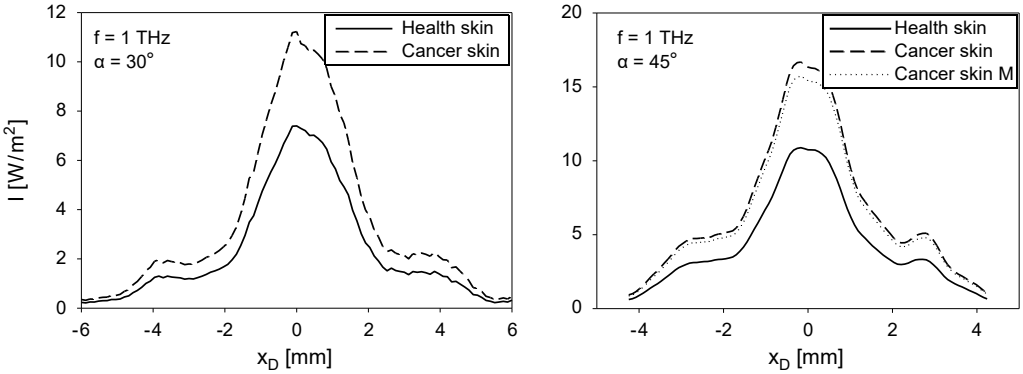

Fig. 6. Distribution of intensity of radiation with $f = 1$ THz with $\alpha = 30°$ and $\alpha = 45°$, as a function of position on the screen, $\Delta = 6 \times 10^{-5}$ m.

The results of measurement depend on parameters such as resolution, noise, and other environmental parameters, such as temperature, relative humidity, *etc*. The resolution of detector can be spatial and spectral. With a detector of smaller dimensions, which corresponds to higher frequency radiation, the resolution is higher, but the intensity of the detected signal is lower. Also, in the case of spectral resolution, there is a frequency response of the instrument, which defines the power of the frequency separation. Noise can additionally affect the measurement value, which is caused by changes in temperature, characteristics of electronic devices, and similar. These are the characteristics of the instrument that is calibrated for the appropriate environmental conditions. In this paper, the distribution of reflected radiation that reaches the detector, at a given distance and at the angles shown in relation to the skin, is given. The response of the device itself depends on the specified parameters, which must be considered during calibration.

The ratio of the intensity of reflected radiation from the cancerous and healthy skin as a function of frequency is shown in Fig. 7. Intensities were shown with angles of 30° and 45°. It could be seen that angle of radiation direction does not influence the ratio of intensities and the maxima is at 0.85 THz.

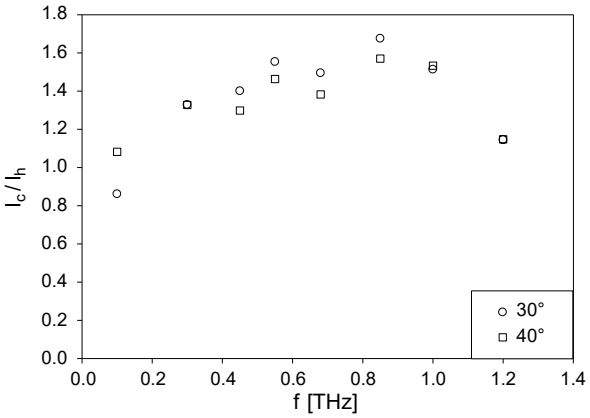

Fig. 7. Ration of intensity of reflected radiation from the cancerous and healthy skin as a function of frequency, for angles of 30° and 45°.

From the presented results it can be observed that the most reflected radiation is at the frequency of $f = 0.85$ THz. It can also be concluded that the absorbed radiation is the largest for 0.1 THz frequency. For that purpose, in Fig. 8 specific absorbed rates for 0.1 and 1 THz were presented. The specific absorbed rate is calculated as $\mathrm{SAR} = \sigma\langle E^2\rangle/\rho$.

The absorbed energy in the skin for THz radiation is smaller than the reflected radiation. This means that the reflected radiation is more suitable for the detection of skin cancer. Absorbed radiation could be used for therapy, but only in very thin skin layers, up to 1 mm in depth.

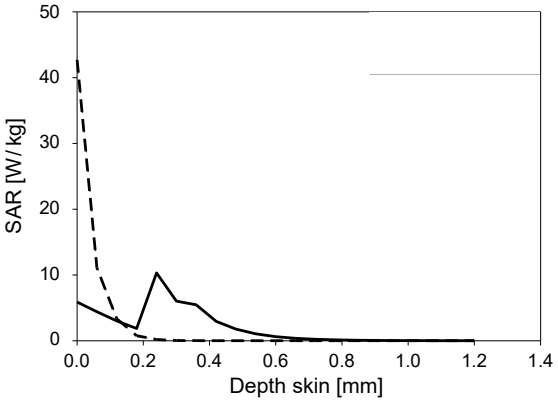

Fig. 8. Specific absorbed energy on the skin for frequencies of 0.1 and 1 THz.

Previous analyses show that high frequency radiation is more reliable and has greater precision, and that the geometry of the radiation does not affect the measurement results. If a higher intensity of reflected radiation is observed during diagnostics, this is a sufficient indicator that the skin has a disease, the nature of which can be established by additional methods. Radiation absorption is at very small depths. Radiation does not penetrate to greater depths and these frequencies are very reliable for diagnosing skin cancer that forms in the surface layers by reflected radiation.

This paper presents the spatial distribution of reflected radiation from the skin. The shape of the distribution of the reflected radiation of the diseased skin is similar to the shape of the distribution of the reflected radiation of the healthy skin, but the intensity is significantly higher for all investigated frequencies. The reason is that electric parameters of cancerous skin have higher values than that for healthy skin. This result was found for other authors [19, 21, 23, 24], whereby cancerous skin has higher values of relative electric constant and conductivity compared to healthy skin. In the paper [26] authors shown that the radiation is absorbed just in the first layer of the stratum spinosum, as shown in this paper.

4. Conclusion

In this paper, THz radiation reflected in the skin was analyzed. The model is based on Maxwell's equations in discrete form (FDTD method).

It was shown that the intensity distributions of reflected radiation are similar for diseased and healthy skin. The radiation intensity is maximal in the center of the distribution and decreases with the distance along the screen. With the increase in frequency, the difference in the intensity of reflected radiation from diseased skin increases up to 1.6 times compared to healthy skin. A similar result was found in [37]. The intensity of reflected radiation is greater for an angle of 45° than for an angle of 30°, as found in [26], but ratio of reflected radiation from cancerous and healthy skin almost does not depend on the radiation angle.

It can be concluded here that the spatial distribution of reflected radiation from healthy and diseased skin is similar for the examined geometries, only differing in the radiation intensity. The biggest difference is at higher frequencies, as confirmed in other papers. In this paper it was found that frequency about 0.85 THz radiation is the most optimal for diagnostic. The distance between skin surface and detector probe should be several centimeters and position and orientation of probe does not influence on result. The dimension of diagnostic probe should not be greater than several millimeters. Environmental conditions in laboratory will be taken into account during calibration of instruments.

This paper is important because the results of our work could be applied to medical science and the development of methodology for skin cancer diagnostics.

The method could be applied for measurement of reflected radiation *in vivo*, by instrument which contains a probe that emits and detects THz radiation. The measurement with instrument in laboratory would be very easy, in real and very short time. Since the distributions of the intensity of reflected radiation from cancerous and healthy skin are similar, the identification consists in measuring the intensity of the reflected radiation. If the intensity is higher, then means that the part of the skin is affected by cancer.

Terahertz radiation is high frequency and enables very reliably diagnostic of cancer in skin in very thin surface layer. Since, distribution of reflected radiation does not depend on geometry, it will not occur as an error in diagnostic. It is very important to note is that the radiation is not absorbed in the deeper layers of the skin and does not damage it. So, from that aspect, this is a reliable and harmless method.

Spatial distribution of reflected radiation can depend on many factors, such as the geometry of the source, the position of the source in relation to the skin, which is defined by the angle and distance, the frequency and polarization of the waves, as well as the structure of the skin. The influence of all these parameters is necessary and it is possible to examine with the FDTD method, which will be our next task.

Acknowledgments

The present paper was supported by The Ministry of Education of the Republic of Serbia (451-03-65/ 2024-03/ 200122).

References

[1] Feldman Y., Puzenko A., Ishai P.B., Caduff A., Davidovich I., Sakran F., Agranat A.J., *The electromagnetic response of human skin in the millimetre and submillimetre wave range*, Physics in Medicine & Biology **54**(11), 2009: 3341-3363. https://doi.org/10.1088/0031-9155/54/11/005

[2] Fenton L.A., Horsfall I., Carr D.J., *Skin and skin simulants*, Australian Journal of Forensic Sciences **52**(1), 2020: 96-106. https://doi.org/10.1080/00450618.2018.1450896

[3] Hwang K., *Surgical anatomy of the upper eyelid relating to upper blepharoplasty or blepharoptosis surgery*, Anatomy & Cell Biology **46**(2), 2013: 93-100. https://doi.org/10.5115/acb.2013.46.2.93

[4] Kanitakis J., *Anatomy, histology and immunohistochemistry of normal human skin*, European Journal of Dermatology **12**(4), 2002: 390-401.

[5] BARONI A., BUOMMINO E., DE GREGORIO V., RUOCCO E., RUOCCO V., WOLF R., *Structure and function of the epidermis related to barrier properties*, Clinics in Dermatology **30**(3), 2012: 257-262. https://doi.org/10.1016/j.clindermatol.2011.08.007

[6] LIM K.-M., *Skin epidermis and barrier function*, International Journal of Molecular Sciences **22**(6), 2021: 3035. https://doi.org/10.3390/ijms22063035

[7] BROWN T.M., KRISHNAMURTHY K., *Histology, Dermis*, StatPearls Publishing, 2022.

[8] MARKS J.G., MILLER J.J., *Lookingbill and Marks' Principles of Dermatology*, 4 Ed., Saunders, Philadelphia, 2006.

[9] OWDA A.Y., SALMON N., HARMER S.W., SHYLO S., BOWRING N.J., REZGUI N.D., SHAH M., *Millimeter -wave emissivity as a metric for the non-contact diagnosis of human skin conditions*, Bioelectromagnetics **38**(7), 2017: 559-569. https://doi.org/10.1002/bem.22074

[10] AMINZADEH R., SAVIZ M., SHISHEGAR A.A., *Dielectric properties estimation of normal and malignant skin tissues at millimeter-wave frequencies using effective medium theory*, 22nd Iranian Conference on Electrical Engineering (ICEE), Tehran, Iran, 2014: 1657-1661. https://doi.org/10.1109/IRANIANCEE.2014.6999804

[11] OWDA A.Y., SALMON N., CASSON A.J., OWDA M., *The reflectance of human skin in the millimeter -wave band*, Sensors **20**(5), 2020: 1480. https://doi.org/10.3390/s20051480

[12] OWDA A.Y., OWDA M., *Early detection of skin disorders and diseases using radiometry*, Diagnostics **12**(9), 2022: 2117. https://doi.org/10.3390/diagnostics12092117

[13] KAUR J., KHAN S.A., *Electric field and specific absorption rate (SAR) analysis in multilayered skin tissue exposed to 5G mobile communication frequencies*, AIP Conference Proceedings **2142**(1), 2019: 110028. https://doi.org/10.1063/1.5122488

[14] SACCO G., PISA S., ZHADOBOV M., *Age dependence of electromagnetic power and heat deposition in near surface tissues in emerging 5G bands*, Scientific Reports **11**, 2021: 3983. https://doi.org/10.1038/s41598-021-82458-z

[15] NARAYANAMURTHY V., PADMAPRIYA P., NOORASAFRIN A., POOJA B., HEMA K., KHAN A.Y.F., NITHYAKALYANIC K., SAMSURI F., *Skin cancer detection using non-invasive techniques*, RSC Advances **8**(49), 2018: 28095-28130. https://doi.org/10.1039/C8RA04164D

[16] SATTLER E., KÄSTLE R., WELZEL J., *Optical coherence tomography in dermatology*, Journal of Biomedical Optics **18**(6), 2013: 061224. https://doi.org/10.1117/1.JBO.18.6.061224

[17] PIERCE M.C., STRASSWIMMER J., PARK B.H., CENSE B., DE BOER J.F., *Advances in optical coherence tomography imaging for dermatology*, Journal of Investigative Dermatology **123**(3), 2004: 458-463. https://doi.org/10.1111/j.0022-202X.2004.23404.x

[18] DELRUE C., SPEECKAERT R., OYAERT M., DE BRUYNE S., SPEECKAERT M.M., *From vibrations to visions: Raman spectroscopy's impact on skin cancer diagnostics*, Journal of Clinical Medicine **12**(23), 2023: 7428. https://doi.org/10.3390/jcm12237428

[19] ZAYTSEV K.I., KUDRIN K.G., KARASIK V.E., RESHETOV I.V., YURCHENKO S.O., *In vivo terahertz spectroscopy of pigmentary skin nevi: Pilot study of non-invasive early diagnosis of dysplasia*, Applied Physics Letters **106**(5), 2015: 053702. https://doi.org/10.1063/1.4907350

[20] ZAITSEV K.I., CHERNOMYRDIN N.V., KUDRIN K.G., RESHETOV I.V., YURCHENKO S.O., *Terahertz spectroscopy of pigmentary skin nevi in vivo*, Optics and Spectroscopy **119**(3), 2015: 404-410. https://doi.org/10.1134/S0030400X1509026X

[21] LI J., XIE Y., SUN P., *Edge detection on terahertz pulse imaging of dehydrated cutaneous malignant melanoma embedded in paraffin*, Frontiers of Optoelectronics **12**, 2019: 317-323. https://doi.org/10.1007/s12200-019-0861-1

[22] GORYACHUK A.A., BEGAEVA V.A., KHODZITSKY M.K., TRULOFF A.S., *The optical properties and spectral features of malignant skin melanocytes in the terahertz frequency range*, Journal of Physics: Conference Series **735**, 2016: 012073. https://doi.org/10.1088/1742-6596/735/1/012073

[23] ZAYTSEV K.I., KUDRIN K.G., RESHETOV I.V., GAVDUSH A.A., CHERNOMYRDIN N.V., KARASIK V.E., YURCHENKO S.O., *In vivo spectroscopy of healthy skin and pathology in terahertz frequency range*,

Journal of Physics: Conference Series **584**, 2015: 012023. https://doi.org/10.1088/1742-6596/584/1/012023

[24] Zhang R., Yang K., Abbasi Q., AbuAli N.A., Alomainy A., *Experimental characterization of artificial human skin with melanomas for accurate modelling and detection in healthcare application*, 43rd International Conference on Infrared, Millimeter, and Terahertz Waves (IRMMW-THz), Nagoya, Japan, 2018: 1-2. https://doi.org/10.1109/IRMMW-THz.2018.8509886

[25] Zhang R., Yang K., Yang B., AbuAli N.A., Hayajneh M., Philpott M., Abbasi Q.H., Alomainy A., *Dielectric and double Debye parameters of artificial normal skin and melanoma*, Journal of Infrared, Millimeter, and Terahertz Waves **40**, 2019: 657-672. https://doi.org/10.1007/s10762-019-00597-x

[26] Vilagosh Z., Lajevardipour A., Wood A.W., *Computational absorption and reflection studies of normal human skin at 0.45 THz*, Biomedical Optics Express **11**(1), 2020: 417-431. https://doi.org/10.1364/BOE.377424

[27] Sullivan D.M., *Electromagnetic Simulation using Finite-Difference Time-Domain Method*, The Institute of Electrical and Electronics Engineering, Inc., New York, 2020.

[28] Lwin Z.M., Yokota M., *Numerical analysis of SAR and temperature distribution in two dimensional human head model based on FDTD parameters and the polarization of electromagnetic wave*, AEU - International Journal of Electronics and Communications **104**, 2019: 91-98. https://doi.org/10.1016/j.aeue.2019.03.010

[29] Alisoy H.Z., Barlaz Us S., Alagoz B.B., *An FDTD based numerical analysis of microwave propagation properties in a skin-fat tissue layers*, Optik **124**(21), 2013: 5218-5224. https://doi.org/10.1016/j.ijleo.2013.03.085

[30] Born M., Wolf E., *Principles of Optics*, Pergamon Press, New York, 1970.

[31] Milosevic M., Stevanovic N., Markovic V.M., Cimbaljevic Z., *Finite difference time domain method of light propagation through inhomogeneous media*, Optica Applicata **53**(4), 2023: 523-538. https://doi.org/10.37190/oa230402

[32] Sasaki K., Mizuno M., Wake K., Watanabe S., *Monte Carlo simulations of skin exposure to electromagnetic field from 10 GHz to 1 THz*, Physics in Medicine & Biology **62**(17), 2017: 6993-7010. https://doi.org/10.1088/1361-6560/aa81fc

[33] Vilagosh Z., Lajevardipour A., Wood A., *Modelling terahertz radiation absorption and reflection with computational phantoms of skin and associated appendages*, Proceedings of the SPIE, Vol. 10456, Nanophotonics Australasia 2017, 2018: 104560M. https://doi.org/10.1117/12.2283206

[34] Vilagosh Z., Lajevardipour A., Wood A., *An empirical formula for temperature adjustment of complex permittivity of human skin in the terahertz frequencies*, Bioelectromagnetics **40**(1), 2019: 74-79. https://doi.org/10.1002/bem.22156

[35] Skocik P., Neumann P., *Measurement of complex permittivity in free space*, Procedia Engineering **100**, 2015: 100-104. https://doi.org/10.1016/j.proeng.2015.01.347

[36] Naqvi S.A.R., Mobashsher A.T., Mohammed B., Foong D., Abbosh A., *Benign and malignant skin lesions: Dielectric characterization, modelling and analysis in frequency band 1 to 14 GHz*, IEEE Transactions on Biomedical Engineering **70**(2), 2023: 628-639. https://doi.org/10.1109/TBME.2022.3199094

[37] Chan K.Y., Ramer R., *Novel concept of detecting basal cell carcinoma in skin tissue using a continuous-wave millimeter-wave rectangular glass filled probe*, Medical Devices: Evidence and Research **11**, 2018: 275-285. https://doi.org/10.2147/MDER.S168338

Received November 30, 2024
in revised form January 29, 2025